Strategies for modeling homogeneous isotropic turbulence and investigation of spatially correlated aerodynamic forces on a stationary model

Jianhan Yu[a,b], Mingshui Li[a*], Ted Stathopoulos[b]

a) Research Centre for Wind Engineering, Southwest Jiaotong University, Chengdu, 610031, China

b) Concordia University, Montreal, Quebec H3G 1M8 Canada,

Abstract: A numerical simulation method is proposed for the generation of homogeneous isotropic turbulence and is applied to the investigation of the spanwise coherence aerodynamic force on a stationary airfoil. First, the inflow turbulence is generated by modeling a grid at the inlet of the computational domain. To verify the accuracy of the generated turbulence field, a series of relevant parameters are compared with the results of wind tunnel tests and previous studies. A model with NACA 0015 profile is then placed in the downstream turbulence. The relationship between the spanwise correlation width of the vertical turbulence component and the lift force is determined. Possible mechanisms for the result are discussed. This study demonstrates that the proposed turbulence generation method is an effective tool for investigating the spatial distribution of unsteady aerodynamic loads on elongated bodies.

Keywords: Numerical simulation; grid-generated turbulence; spatial distribution; aerodynamic force.

---

* Corresponding author.
Email address: lms_rcwe@126.com (Mingshui Li)

1. Introduction

Almost all previous studies of spatially correlated aerodynamic forces on bodies immersed in turbulent flow have involved wind tunnel tests or theoretical analyses. In contrast to these approaches, numerical methods have the advantage of providing abundant detailed data at low cost. In recent years, with the rapid development of both computational fluid dynamics (CFD) techniques and computer hardware, several numerical methods for generating turbulence using large eddy simulation (LES) have been proposed to model the characteristics of real fluid flows. The generation of turbulence by CFD software has great potential for the investigation of the three-dimensional characteristics of aerodynamic forces.

For accurate simulation of aerodynamic forces on bodies immersed in turbulent flows, the generated turbulence field must, like a real flow, be spatially correlated and evolved. Also, for engineering application, the turbulence parameters must be easily modified. There are two main methods for generating homogenous isotropic turbulence at the inlet of the computational domain using LES: precursor simulation (Spalart, 1986, 1988; Pierce and Moin, 1998; Schlüter and Moin, 2004; Jiang, et al., 2012) and the synthesis method (Lee et al., 1992; Kondo et al., 1997; Mathey et al., 2006; Huang et al., 2010). The two methods have been reviewed in detail by Liu and Pletcher (2006), Tabor (2010), and Dhamankar (2015). Both methods specify the statistical data character of instantaneous turbulence as part of the inlet boundary conditions. Synthesis methods are convenient to specify the parameters of the inlet turbulence, but they are inherently inaccurate and the provision of an inlet development section is required. In contrast, precursor simulation methods generate true turbulence that is inherently more accurate, however can be cumbersome to generate the turbulence of required characteristics. In this study, a method of directly modeling the grid at the inlet to generate spatially correlated and evolved turbulence is proposed. The advantage of this grid-generated turbulence method is the generation of inherently accurate turbulence that allows easy comparison with wind tunnel tests; as well, the turbulence characteristics can be modified conveniently by changing the size of the grid.

In the study of unsteady aerodynamic loading on elongated bodies in turbulent flows, one of the fundamental assumptions is the strip assumption, according to which the spatial distribution of unsteady aerodynamic loading can be represented by oncoming transversely fully coherent gusts (Fung, 1955). This assumption had been widely adopted in wind loading codes and standards. However, as first observed by Nettleton (see Ektin, 1971), the lift force on an airfoil is more strongly correlated than the fluctuation components when the turbulence scale is smaller than or similar to the chordwise dimension of the airfoil, thus invalidating the strip assumption. Nettleton's finding has been confirmed by wind tunnel tests relating to the lift force on a bluff body (Sankaran and Jancauskas, 1993; Jakobsen, 1997; Kimura et al., 1997; Larose, 1997; Li, 2015).

All previous research on this topic involved either theoretical analysis or wind tunnel tests, whereas, in the present study, the relationship between vertical velocity fluctuations and unsteady aerodynamic loading is investigated through CFD simulations. First, a grid is modeled at the inlet of the computational domain to generate homogeneous isotropic turbulence, using three-dimensional LES. After verification of the simulation results by comparison with the results of wind tunnel tests and previous studies, a stationary model of a section of the NACA 0015 airfoil is chosen to study the spatial correlation of aerodynamic forces. A relationship between the spanwise correlation width of the vertical velocity fluctuation and the lift force is obtained and an argument regarding the strip assumption is presented. Finally, the results are discussed.

It should be emphasized that the spanwise correlation width of the vertical velocity component and the lift force, which are obtained primarily by numerical methods in this study, are essential for further investigations such as identification of the three-dimensional aerodynamic admittance of elongated bodies like the decks of long-span bridges.

2. Turbulence generation method

The grid-generated turbulence is produced by modeling a pattern of solid patches at the inlet of the computational domain as in the wind tunnel test. Fig. 1 shows the setup of the inlet grid pattern in this study. Four inlet grids are used to generate turbulence. An inlet grid size M = 0.04 m and a bar size of 0.007 m are chosen to facilitate comparison with the wind tunnel test results of Li (2015) to verify the accuracy of the simulation results. The dimension of the computational domain is scaled down by a factor of 10 compared with experiment. This scaling is a balance between the two factors. On the one hand, a small mesh size is required to capture the small-scale vortices to allow investigation of the influence of high-frequency turbulent fluctuations on the aerodynamic force on the structure. On the other hand, if the mesh is too fine, then computational efficiency will be poor or computational capabilities will be exceeded. With this scaling, it is possible to achieve a consistent influence of turbulence on bodies in the simulations and in the wind tunnel tests by choosing the same Reynolds number, while also improving the computational efficiency. The experiments are described in Section 3.

The computational domain is shown in Fig. 2. Both the height and width of the domain are 4 *M* and the length is 60 *M*. This length is chosen to allow investigation of the development of the turbulence field and the relationship among the various parameters involved. The CFD simulations are described in Section 4 and the validation of the generated turbulence field is described in Section 5.

The proposed method can be used to study the aerodynamic characteristics of a body by placing it in the nearly isotropic and homogenous region downstream of the inlet. The use of this method to investigate the spanwise coherence characteristics of the aerodynamic force on a body is described in Section 6.

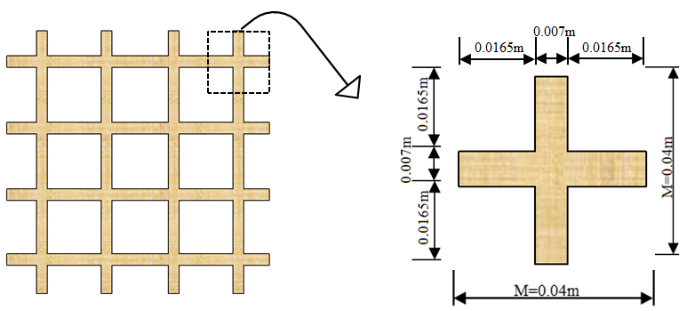

Fig. 1. Grid inlet.

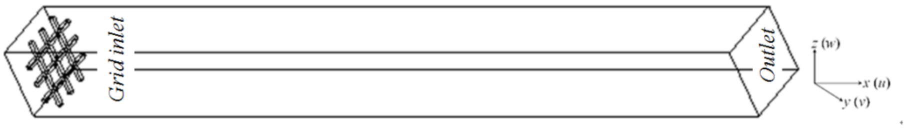

Fig. 2. Computational domain.

3. Experimental setting

A wind tunnel test conducted by Li (2015) is chosen to verify the numerical simulation method proposed in this study. The experiment was carried out in the high-wind-speed test section of the XNJD-1 wind tunnel at Southwest Jiaotong University. A uniform grid was placed at the inlet to produce a homogeneous isotropic turbulence field (Fig. 3). The grid aperture was 0.33 m and the bar size was 0.07 m. The inlet grid consists of 4 × 4 = 16 grid patterns. The turbulent fluctuations were measured simultaneously in the streamwise, spanwise, and vertical directions by a Cobra Probe downstream at the position where the model airfoil to be investigated would be placed. The turbulence integral scale and turbulence intensity in the three directions at the model location are shown in Table 1.

Fig. 4 compares the experimental results for the spanwise correlation coefficients of the vertical fluctuation component with the theoretical results of Bullen (1961). It can be seen that the measured correlation coefficients of the vertical velocity fluctuation are in agreement with Bullen's results, which means that the turbulence generated in the wind tunnel test satisfies the assumption of homogeneity and isotropy. The test results are thus highly reliable and can be used for comparison.

Fig. 3. Wind tunnel test of Li (2015).

Table 1 Parameters of grid-generated turbulence in wind tunnel test.

Turbulence integral scale			Turbulence intensity		
L_u (m)	L_v (m)	L_w (m)	I_u (%)	I_v (%)	I_w (%)
0.107	0.042	0.054	8.0	6.1	6.5

Note: L_u, L_v, and L_w are the streamwise, spanwise, and vertical integral scales, respectively; I_u, I_v, and I_w are the streamwise, spanwise, and vertical turbulence intensities, respectively.

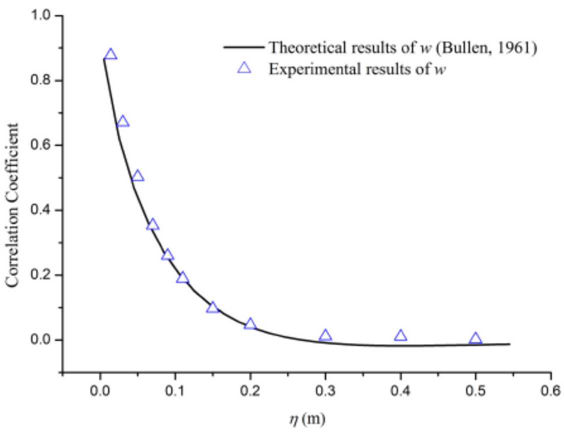

Fig. 4. Spanwise correlation coefficients of *w*: comparison between experimental results and Bullen's theoretical results (After Li, 2015).

4 Numerical methods

4.1 Turbulence modeling and solver setting

In this study, a three-dimensional incompressible fluid motion is described using LES, in which the large-scale turbulence is resolved while small-scale turbulence is modeled. The commercial CFD code FLUENT 6.3 is adopted to solve the fluid governing equations of LES. The filtered unsteady Navier–Stokes equations are as follows:

$$\frac{\partial \bar{u}_i}{\partial x_i} = 0 \tag{1}$$

$$\frac{\partial \bar{u}_i}{\partial t} + \frac{\partial \bar{u}_i \bar{u}_j}{\partial x_j} = -\frac{1}{\rho}\frac{\partial p}{\partial x_i} + \frac{\partial}{\partial x_j}\left[(\nu + \nu_{\mathrm{SGS}})\frac{\partial \bar{u}_i}{\partial x_j}\right] \tag{2}$$

where $\bar{u}_i$ (i = 1, 2, 3) are the velocity components in the three coordinate directions, x_i (i = 1, 2, 3) are the displacements in these three directions, ρ and p are the air density and pressure, ν is the kinematic viscosity, ν_{SGS} is the subgrid-scale viscosity, and the overbar indicates spatially filtered components.

A filter function is used to split the turbulent flow into subgrid-scale (SGS) and grid-scale (GS) components. The Smagorinsky model is adopted to describe the SGS stresses between the GS and SGS eddies. The filter function and the Smagorinsky model are given by

$$\nu_{\mathrm{SGS}} = (C_S \Delta)^2 \sqrt{2\bar{S}_{ij}\bar{S}_{ij}} \tag{3}$$

$$\bar{S}_{ij} = \frac{1}{2}\left(\frac{\partial \bar{u}_i}{\partial x_j} + \frac{\partial \bar{u}_j}{\partial x_i}\right) \tag{4}$$

where ν_{SGS} is the SGS eddy viscosity, $\bar{S}_{ij}$ is the strain rate tensor, $\Delta = \sqrt[3]{\Delta x \Delta y \Delta z}$ is the grid filter width and C_S is the Smagorinsky constant coefficient.

In the present investigation, the value of Smagorinsky constant is taken as $C_S = 0.1$, which is an appropriate value for the simulation of bodies immersed in turbulent flow (Liang and Papadakis, 2007). The FLUENT code is based on the finite-volume method (FVM), which defines the pressure and velocity at the centers of the control volumes and the volume fluxes at the midpoints of the cell surfaces. The well-known PISO (pressure implicit with splitting of operators) algorithm proposed by Issa (1986) is used for the pressure-velocity coupling procedure between the momentum and continuity equations. A fully implicit second-order time-advancement scheme is used for temporal discretization to reduce numerical diffusion. To obtain an accurate simulation, a second-order central differencing scheme is chosen for spatial discretization.

4.2 Computational domain and boundary conditions

The geometry of the grid and domain configurations is as shown in Section 2. The computational domain has dimensions of 0.16 m (width) × 0.16 m (height) × 2.4 m (length), where the width and height are scaled down from the wind tunnel cross-section by a factor of 10.

The velocity inlet condition is applied at the inlet boundary with an oncoming flow velocity of 11.5 m/s, which coincides with that of the wind tunnel test. At the outflow boundary, a convection boundary condition is applied for the velocity and a Neumann-type condition for the pseudo-pressure. A no-slip boundary condition ($u = v$

= w = 0) is imposed at the wall and on the grid surface, which again is similar to the conditions in the wind tunnel experiment.

4.3 Grid-independence test

The accuracy of the computational simulation results depends strongly on the cell numbers and mesh size, and so the grid-independence test is extremely important. Given the simplicity of the model structure, hexahedral cells are employed in the simulation to obtain stable algorithms and accurate account of viscous effects. Small mesh size is required to capture the small-scale vortices. However, an excessive number of cells will reduce computational efficiency. To test the influence of mesh size, the turbulence intensity and spanwise correlation relationship of vertical turbulence are compared with Li's wind tunnel test results. The mesh sizes are uniformly spaced along the streamwise, spanwise, and vertical directions. Three mesh sizes are tested: 0.00625 m, 0.003125 m, and 0.001875 m. The velocity data of 10 seconds physical time is used in order to have a long enough statistical sample to obtain the spanwise correlation coefficient. Computations are carried out on 8 Intel Core i7-7820X 3.6GHz CUPs with 16 threads parallel computing. The maximum of about 16 G of RAM memory is required. The number of cells and calculation time of the three cases are specified in Table 2.

Table 2 Number of cells and computational time

Case	Mesh size (m)	Number of cells (million)	Computational time (days)
1	0.00625	0.92	1
2	0.003125	3.59	4
3	0.001875	10.69	11

Comparisons of turbulence intensity components are shown in Table 3. In general, the results of I components in all three cases are in good agreement with those of the wind tunnel test. The accuracy improves with decreasing the cells size. There is a large deviation of case 1 but that of cases 2 and 3 is relatively small, although there is a higher discrepancy for the prediction of the spanwise turbulence intensity with case 3 than with case 2 which however involves a coarser mesh. This may be due to the error of wind tunnel experiment.

Table 3 Grid-independence test of turbulence intensity.

Case	Mesh size (m)	I_u (%)	I_v (%)	I_w (%)	Deviation in I_u (%)	Deviation in I_v (%)	Deviation in I_w (%)
1	0.00625	7.51	6.52	5.92	6.13	6.89	8.92
2	0.003125	7.85	6.16	6.22	1.88	0.98	4.31
3	0.001875	7.96	5.96	6.33	0.50	2.30	2.62

The relationships among L components in the streamwise, spanwise, and vertical directions are important criteria to test the authenticity of homogeneous isotropic turbulence fields. The results are shown in Table 4. Again, the results improve with the decreasing of mesh size. However, agreement is less satisfactory for the relationships among the L components, with the coefficients of proportionality obtained by numerical simulation being somewhat higher than those from the wind tunnel test: by 11% - 17% for the relationship between the vertical and streamwise components and as much as 27% - 34% for that between the spanwise and streamwise components. This latter deviation may be due to experimental error since the value of L_v obtained by wind tunnel test is relatively small compared with theoretical value.

Table 4 Grid-independence test of turbulence integral length-scale.

Case	Mesh size (m)	L_v/L_u	L_w/L_u	Deviation in L_v/L_u	Deviation in L_w/L_u
1	0.00625	0.528	0.594	34%	17%
2	0.003125	0.505	0.578	28%	14%
3	0.001875	0.497	0.561	27%	11%

Six observation points with uneven spacing, as shown in Fig. 5, are chosen at the central line of the cross section 45 M downstream of the inlet grid to determine the correlations among vertical turbulence fluctuations. A comparison of the spanwise correlation results of numerical simulation with those of the wind tunnel test is shown in Fig. 6. The result improves with the refinement of the mesh, cases 2 and 3 are both consistent with the wind tunnel test result, while the coefficients in case 1 are slightly higher than the test result at smaller distances.

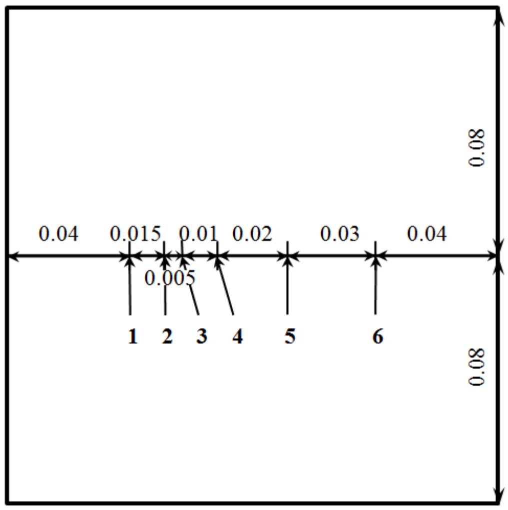

Fig. 5 Distribution of observation points – distances are in meters

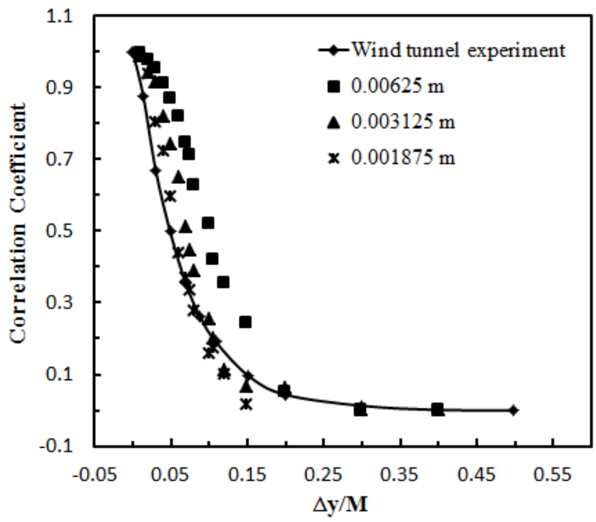

Fig. 6. Grid-independence test of the spanwise relationship.

On the basis of the grid-independence test, a cell size of 0.003125 m is adopted to capture the turbulent field characteristics adequately while saving computational time. The mesh distribution is shown in Fig. 7. The first layer of mesh size near the surface of the grid is 0.00003 m, with corresponding values of $y^{+} \leq 1$. The wall – resolved LES is adopted to obtain an accurate simulation of the boundary layer. The high aspect ratio is avoided by scaling down the computational domain size and increasing the cells number. The dimensionless cell sizes of the model surface are $\overline{\Delta x^{+}} = 41$,

$\overline{\Delta y^{+}} = 80$, where x and y are streamwise and spanwise respectively. It is worth pointing out that these values are larger than those suggested for wall-resolved LES, namely $\Delta x^{+} = 100$, $\Delta y^{+} = 20$ by Chapman (1979) and $\Delta x^{+} = 50 \sim 130$ and $\Delta y^{+} = 15 \sim 30$ by Choi and Moin (2012). However the adopted mesh generation strategy permits to achieve a sufficiently good result with an overall cells number of about 3.59×10^{6}.

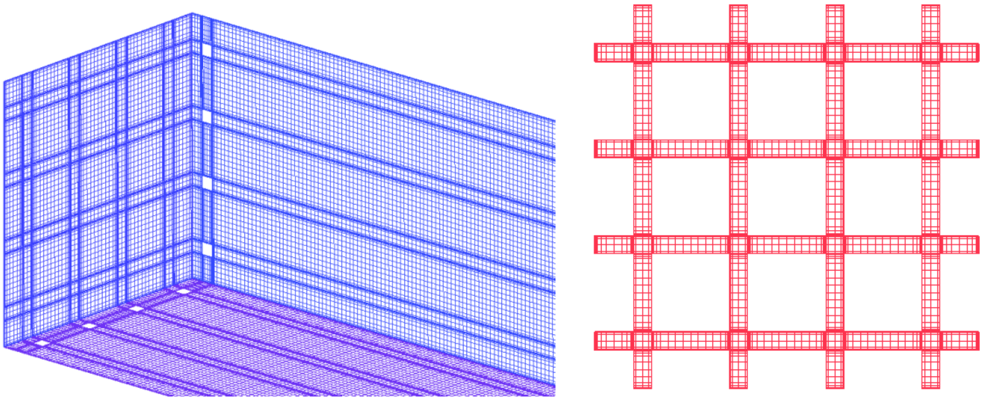

(a) (b)

Fig. 7. Computational mesh distribution: (a) computational domain; (b) mesh of inlet grid.

5. Validation of turbulence field

In order to demonstrate that the proposed turbulence generation method can be used effectively to investigate the aerodynamic characteristics of structures, the turbulence should satisfy the following conditions:

(1) the development of vortex structures should exhibit behavior like that of real grid-generated turbulence;

(2) a series of relevant turbulence parameters should be validated to ensure that a nearly homogeneous isotropic region is obtained downstream.

In this section, a series of relevant turbulence parameters are compared with wind tunnel results and the results of previous studies to verify the accuracy of the numerical simulation results. The parameters to be verified are the power-law relationship of turbulence intensity and integral length-scale, the wind spectral density, and the spatial correlation relationships of the turbulence.

5.1 Power-law relationship

The instantaneous vortex structures of the turbulence field generated by numerical methods are shown in Fig. 8. A deeper insight into the structure of the turbulent flow in the interior of the domain can be obtained from Figs. 9 and 10. Fig. 9 displays the magnitude of the vorticity in an *xz* cutting plane in the middle of the simulation domain (y = 2 M), while Fig. 10 displays the magnitude of the vorticity in *yz* cutting planes (i.e., planes parallel to the grid) at distances x = 5 M, 10 M, 15 M, 20 M, 25 M, 30 M, 35 M, and 40 M downstream of the computational domain.

It can be seen that the development of the turbulence field downstream of the inlet is identical to the description of a wind tunnel result given by Monin and Yaglon (1975), who proposed that the turbulence field downstream of a grid can be divided into three regions. The first region, which is next to the grid, is called the developing region. The vorticity is generated at the grid of the inflow boundary and develops into the domain from there. This region consists mainly of the grid wakes. It can be seen clearly from Fig. 1 (a–d) that the flow is non-homogeneous and anisotropic.

The turbulence gradually become homogenous and isotropic as the flow proceeds downstream, as can be seen from Fig. 10 (e-h), although there is apparently energy transfer between wavenumbers. In the near-wall region, the turbulence develops into elongated streamwise structures, while more homogeneous, isotropic turbulence is generated away from the wall. Aerodynamic effects on bodies immersed in a turbulent flow are usually investigated in this region. This region is followed by the developed region which is the final period of decay. Figures 8–10 demonstrate that the method presented here enables simulation of more realistic flow structures.

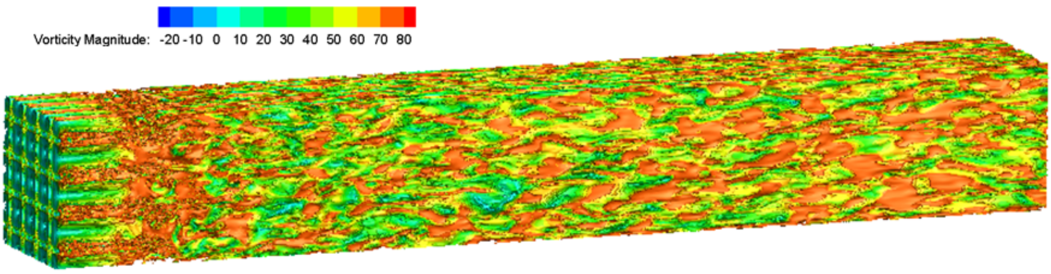

Fig. 8. Development of instantaneous vortex structures.

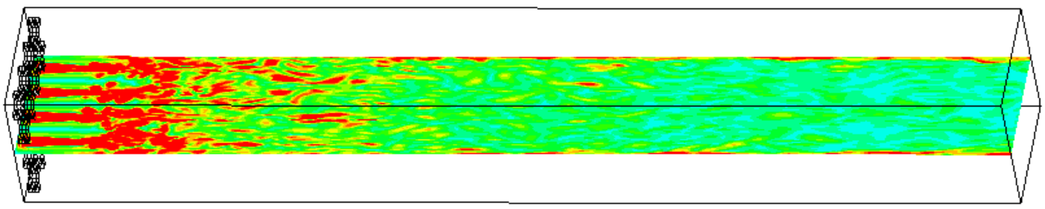

Fig. 9. Contours of instantaneous vorticity in the *xz* plane at $y = 2\ M$.

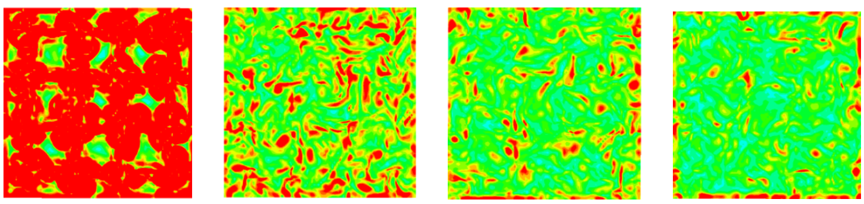

(a) (b) (c) (d)

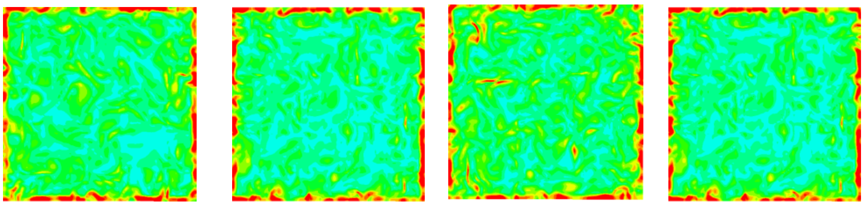

(e) (f) (g) (h)

Fig. 10. Contours of instantaneous vorticity in *yz* planes at (a) $x = 5\ M$; (b) $x = 10\ M$; (c) $x = 15\ M$; (d) $x = 20\ M$; (e) $x = 25\ M$; (f) $x = 30\ M$; (g) $x = 35\ M$; (h) $x = 40\ M$.

The second region is also called the power-law region, where the decay rate of the turbulence intensity and the growth rate of the integral length both obey power laws. The exponents in these power laws are independent of Reynolds number, grid solidity, rod shape, and mesh size. In a pioneering paper, Taylor (1935b) proposed that the turbulence downstream is statistically homogeneous and approximately isotropic in the power-law region, which is 40 – 50 times the grid length downstream of the grid inlet. It was also suggested by Corrsin (1963) that homogeneity conditions are satisfied at $x/M \geq 40$ for grids with relatively low solidity. In this study, the data from $x/M = 40$ to $x/M = 55$ are used to determine the power-law exponents for the variation of relevant parameters with distance. A series of monitoring points are located on the central line of the computational domain in the streamwise direction to observe the velocity fluctuations.

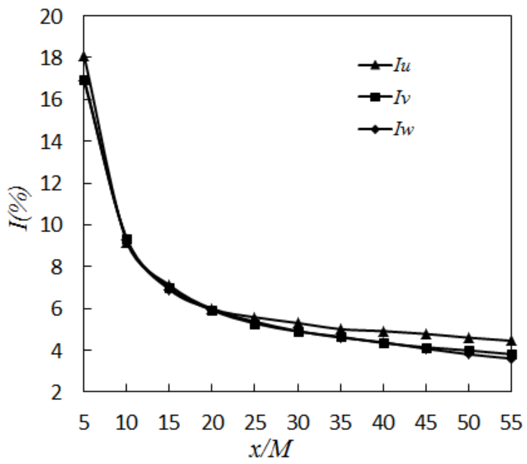

Fig. 11. Development of turbulence intensity with distance from grid inlet.

The development of the turbulence intensity with the distance from the grid inlet is shown in Fig. 11. It can be seen that the intensity falls dramatically from its original value until about 30 *M* downstream of the grid inlet, after which the decrease becomes more gradual between 35 *M* and 55 *M*, which is the nearly homogenous and isotropic region. A decay power law proposed by Mohamed and LaRue (1990) is used to determine the value of the exponent in this investigation, which is based on Taylor's hypothesis:

$$u'^2 / U^2 = I^2 = A\left(x/M - x_0/M \right)^{-n} \tag{5}$$

where u' is the resolved velocity fluctuation in the streamwise direction, U is the mean velocity, A is a constant called the decay coefficient, x is the positive distance downstream of the grid, x_0 is the virtual origin, and n is the decay exponent.

The decay exponent of the turbulence intensity is found by the numerical method to be $1.09 < n < 1.26$ when the virtual origin is taken to be zero. For comparison, the predictions for the decay exponent by von Kármán and Howarth (1938), Kolmogorov

(1941), Saffman (1967), and Mohamed and LaRue (1990) are 1, 1.43, 1.2, and 1.33, respectively.

Another important parameter is the growth exponent for the integral length-scale. With the development of the turbulence field, the integral length-scale first experiences a sharp rise, followed by a more gradual increase as the distance downstream of the grid increases, as displayed in Fig. 12. The power-law relationship is

$$L = B\left(\frac{x - x_0}{M}\right)^m \tag{6}$$

where B is a constant and m is the growth exponent of the length-scale. According to the proposed method, the growth rate in Eq. (6) is $0.376 < m < 0.421$, which corresponds very closely to the values of $m = 0.36$ found by Davidson and Krogstad (2009) and $m \approx 0.4$ found by Krogstad and Davidson (2011).

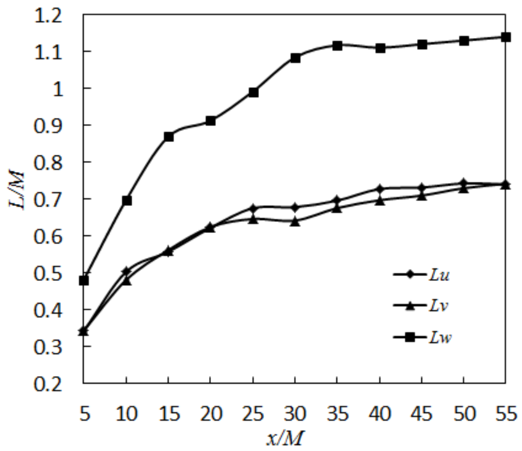

Fig. 12. Development of integral length-scale with distance from grid inlet.

In conclusion, the development of the turbulence intensity and integral length-scale of the generated turbulence field both satisfy power-law relationships. These results demonstrate that the region used to investigate aerodynamic effects on immersed structures meets the condition of a nearly homogeneous and isotropic turbulence field.

5.2 Turbulence spectrum

It is of great importance that the spectrum of the generated turbulence satisfies the von Kármán model (Simiu and Scanlan, 1996), since this model has been found to be appropriate for the real turbulence spectrum in the atmospheric boundary layer (Lumley and Panofsky, 1964; Hinze, 1975; Li et al., 2007) as well as for the homogeneous isotropic turbulence generated by a uniform grid (Robert and Surry, 1973). The spectral densities in the streamwise, spanwise, and vertical directions at the modeling position are shown in Fig. 13. The spectral densities of the generated turbulence are depicted well by the von Kármán spectral model, as expressed by the following equations:

$$\frac{fS_u(f)}{{\sigma_u}^2} = \frac{4\left(\frac{fL_u}{U}\right)}{\left[1+70.8\left(\frac{fL_u}{U}\right)^2\right]^{5/6}} \tag{7a}$$

$$\frac{fS_i(f)}{\sigma_i^2} = \frac{4\left(\frac{fL_i}{U}\right)\left[1+755\left(\frac{fL_i}{U}\right)^2\right]}{\left[1+238\left(\frac{fL_i}{U}\right)^2\right]^{11/6}} \quad (i = v, w) \tag{7b}$$

where f is the turbulence frequency in the streamwise direction, $S_u(f)$, $S_v(f)$, and $S_w(f)$ are the spectra of the fluctuations in the streamwise, spanwise, and vertical directions, respectively, and σ_u, σ_v, and σ_w are the variances of these fluctuations.

As can be seen from Fig. 13, the energy-containing subrange of the turbulence matches well with the von Kármán spectrum model, but the high-frequency part of the inertial subrange and the dissipation subrange are missing. This is a consequence of the characteristics of the LES turbulence model. Eddies with a length-scale greater than the cutoff width are resolved, while smaller turbulent eddies with high frequencies are destroyed and must be described by an SGS model. There will, therefore, be a filter cutoff frequency, which is the point at which the spectral curve deviates from the −5/3 exponent. It can be seen from Fig. 12 that the cutoff frequency in this investigation is about 400 Hz and higher frequencies are no longer resolved. It should be noted that the absence of higher frequencies does not influence the aerodynamic forces to be studied further on in this investigation.

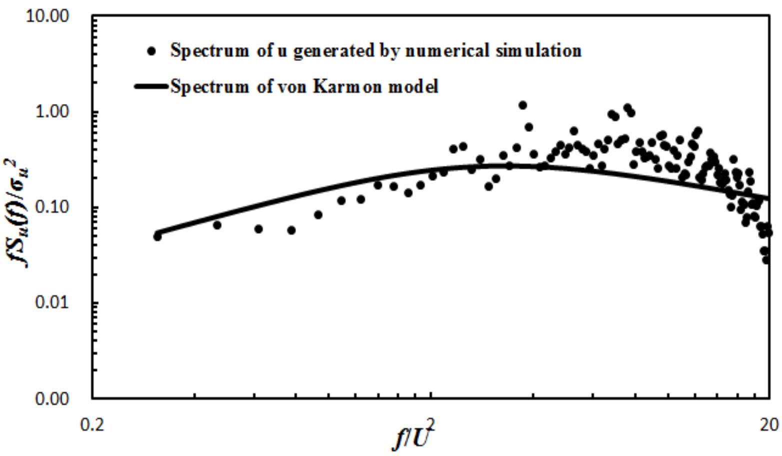

(a)

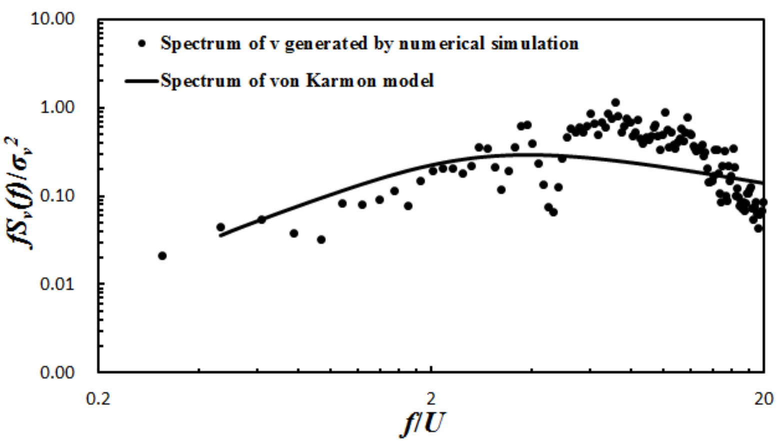

(b)

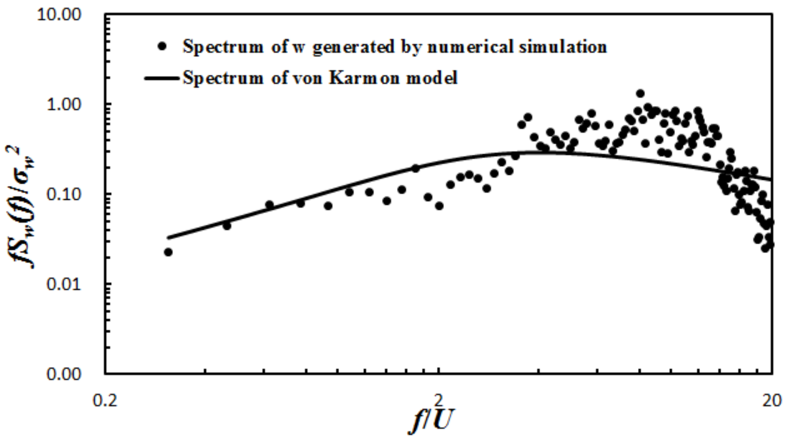

(c)

Fig. 13. Comparisons of spectrum density generated by numerical simulation and von Kármán model: (a) streamwise direction; (b) spanwise direction; (c) vertical direction.

5.3 Spatial correlations

Accurate simulation of spatial correlations is essential in order to provide a correct representation of the self-preservation of the turbulent flow, as well as for investigation of the buffeting lift on bodies immersed in the flow field. Correlation curves from the numerical simulation and the wind tunnel test are shown in Fig. 14. It can be seen that the numerical results correspond well to those from the wind tunnel test, although they do not match precisely. The rate at which the vertical turbulence fluctuation correlation coefficients decrease with distance is somewhat faster in the numerical results than in the experimental results, which means that the generated turbulence is more spatially correlated. This may due to the scaling down of the computational domain in the numerical approach.

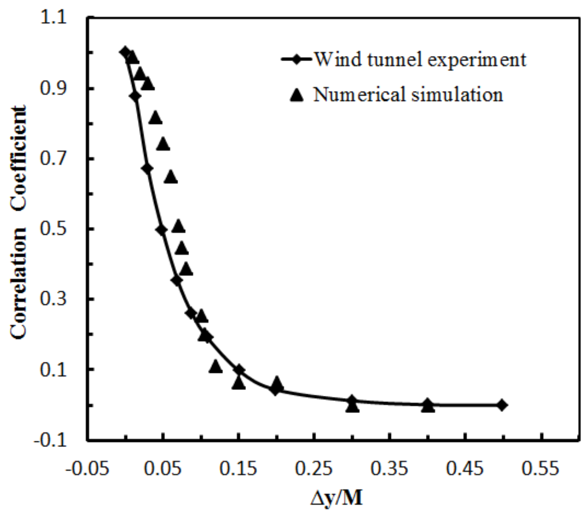

Fig. 14. Comparison of spatial correlations.

6. Investigation of aerodynamic force

6.1 CFD setup

A prism with the NACA 0015 airfoil section is used to investigate the relationship between the coherence of the vertical velocity fluctuations and coherence of the lift force on a slender body. The computational domain is illustrated in Fig. 15. The model is placed 45 M downstream of the inlet grid where the turbulence is nearly homogeneous and isotropic. The Reynolds number at the model position is 66000 and the viscous effects have been considered. The span width of the model is the same as the width of the computational domain. The chord length of the model is 1.25 M and the incidence is 0^{o}. A no-slip boundary condition is imposed on the airfoil surface.

The mesh distribution is shown in Fig. 16. Hexahedral cells are employed in the computational domain. The mesh is equally distributed in the spanwise direction, with a length of 0.004 m. The first layer size above the airfoil surface is 0.00003 m to meet the requirement that $y^{+} \leq 1$. In the computational domain, 4.25 million cells are generated. The whole simulation requires 5 days of computational time.

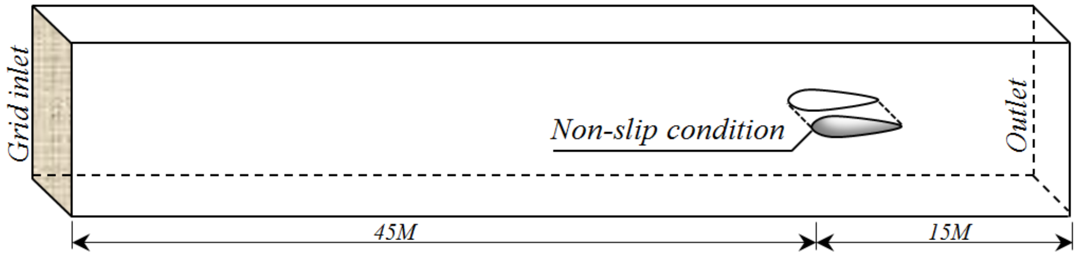

Fig. 15. Computational domain and boundary conditions.

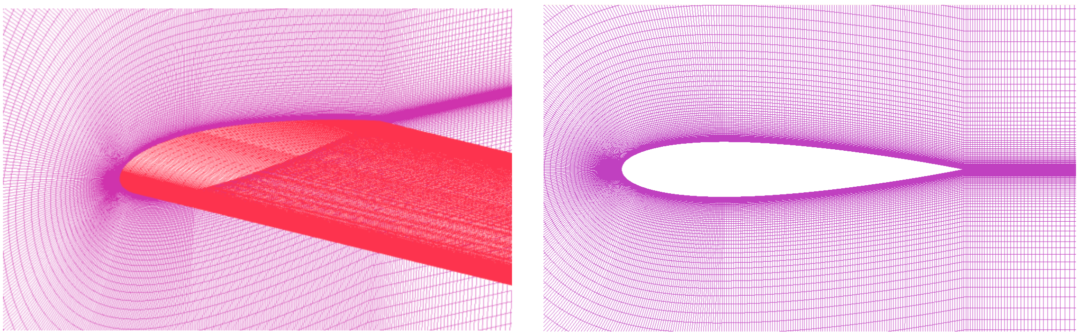

(a) (b)

Fig. 16. Computational mesh distribution: (a) mesh of airfoil; (b) mesh in *xz* plane.

6.2 Results and discussion

The coherence of the buffeting lift is obtained by integrating the unsteady surface pressure around several spanwise spaced strips on the airfoil model. The vertical velocity fluctuations are obtained at several observation points in the empty turbulence field at the central line of airfoil. The distribution of the strips and points is the same with Fig. 5.

The time histories of integrated lift on second and forth strips are shown in Fig. 17. The mean values are close to zero, as the incidence of the airfoil is 0º. The spanwise correlations of buffeting lift and the vertical velocity fluctuation from the numerical simulation are shown in Fig. 18. It is clear from the figure that the buffeting lift is more strongly correlated than the vertical turbulence component. To further examine the correlation relationship between the buffeting lift and the vertical velocity fluctuation, the spanwise correlation width proposed by Larose (1997) is used:

$$L_w^z = \int_0^b R_{12}(\Delta y) d\Delta y \quad (8)$$

where R_{12} is the spanwise correlation function of the random variables at two points and b is the maximum spanwise spacing. By integrating the correlation curves from Fig. 18, the relationship is found to be $L_L^z = 3.17L_w^z$, where L_L^z and L_w^z are the spanwise correlation widths of the buffeting lift and vertical velocity fluctuation, respectively. The result obtained in this study is close to the results obtained by Nettleton (Larose 1997) and Li (2015) from wind tunnel tests, which are $L_L^z = 3.6L_w^z$ and $L_L^z = 3.9L_w^z$, respectively.

This result shows that the strip assumption that uses the spatial distribution of turbulence fluctuations to describe the spatial correlation of the buffeting lift is incorrect. In this study, the chord length of the model is 0.05 m, which is greater than the integral length-scale of the vertical turbulence fluctuation (L_w = 0.023 m). It corresponds to the condition proposed by Nettleton (see Etkin, 1971), according to which the strip assumption fails if the chord length of the body is close to or greater than the integral length-scale of the vertical turbulence component.

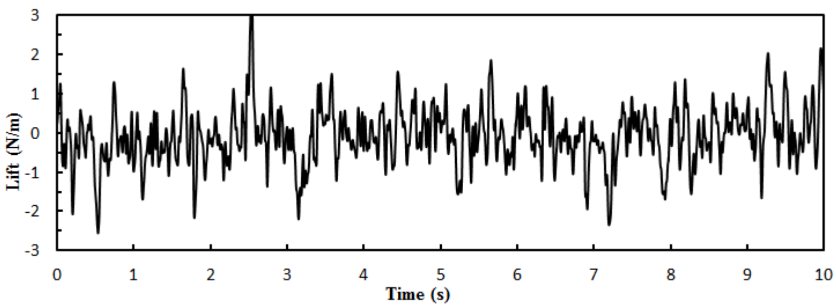

(a)

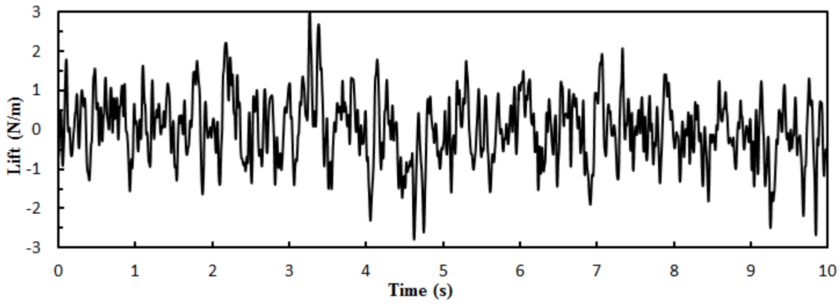

(b)

Fig. 17. Time histories of integrated lift: (a) strip 2; (b) strip 4.

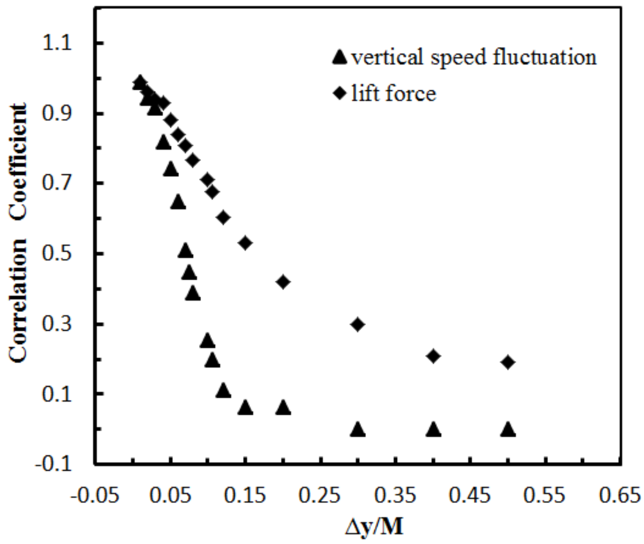

Fig. 18. Spanwise correlation relationship.

Fig. 19 shows the magnitude of the instantaneous vorticity in *yz* cutting planes at different airfoil positions. It is apparent that when the turbulence approaches the airfoil, the presence of the solid wall will modify the structure of the turbulence field. It can be seen from the figure that the turbulence kinetic energy produced by the variation of streamwise and vertical velocities close to the airfoil would follow a two-dimensional pattern, consequently the turbulent flow field around the airfoil may be closer to the two-dimensional (compared to the three-dimensional) background turbulence, which may yield a lift force more correlated than the velocity fluctuation.

Then, after passing through the airfoil, the flow structure will be three-dimensionalized again by the isotropic background turbulence.

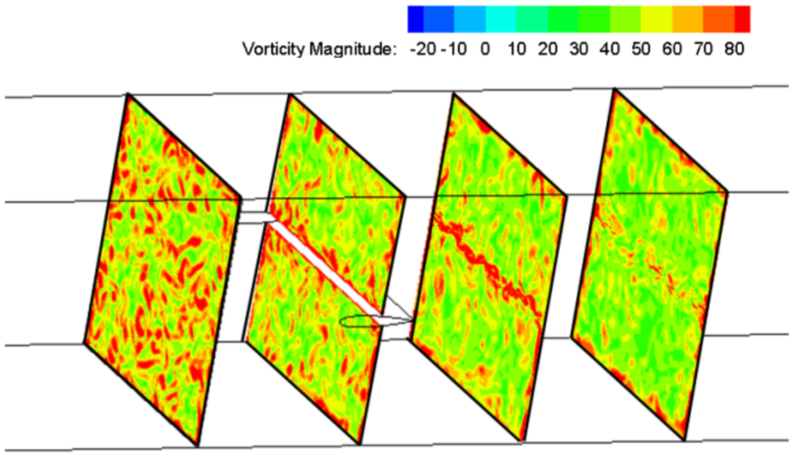

Fig. 19. Contours of instantaneous vorticity in *yz* planes at model positions $x = 43\ M$, $46\ M$, $49\ M$, and $52\ M$.

To the best of the author's knowledge, this is the first time that this relationship has been obtained via a numerical method. It can be concluded that the proposed method for the generation of homogeneous isotropic turbulence provides high accuracy in estimating the spatial distribution of the aerodynamic forces on a body immersed in a turbulent flow, which is of great significance for investigations of the influence of turbulence on such bodies.

7. Conclusion

A new method for generating homogeneous isotropic turbulence by modeling a grid at the inlet of the computational domain has been proposed. The generated turbulence field has been compared with the results of a wind tunnel test and of previous research for the purpose of verification. The conclusions from this comparison can be summarized as follows:

(1) With regard to the development of the turbulence field, the turbulence intensity decay exponent is found to be $1.09 < n < 1.26$ and the length-scale growth rate is found to be $0.376 < m < 0.421$.

(2) The spectra of the three fluctuation components fit the von Kármán spectrum. The filter cutoff frequency is sufficiently high for the investigations in this study.

(3) The spatial correlations among the vertical turbulence fluctuations fit well with the wind tunnel test results.

After the verification of the generated turbulence, a model body with NACA 0015 airfoil section was placed in the computational domain to determine the spatial distribution of the aerodynamic lift force. The relationship between the spanwise correlation width of the buffeting lift and the vertical turbulence fluctuation obtained in this study is $L_L^z = 3.17 L_w^z$. These results show that the strip assumption is invalid.

This paper has demonstrated that the proposed passive grid-generated turbulence method can be used to investigate the spatial distribution of aerodynamic forces on slender bodies immersed in turbulent flows. However, one drawback of this method is that, in general, it incurs a high computational cost, although this may be reduced with the development and improvement of computer hardware.

Acknowledgments

This research was funded in part by the National Natural Science Foundation of China (No. 51478402). The first author would like to acknowledge the associated support services at Concordia University in the completion of this work and the Chinese Scholarship Council (CSC) foundation for providing the financial support to study abroad.

Reference

Batchelor, G. K. (1954). The theory of homogeneous turbulence. Cambridge university press.

Bearman, P. W. (1972). Some measurements of the distortion of turbulence approaching a two-dimensional bluff body. Journal of Fluid Mechanics, 53(3), 451-467.

Bullen, N. I. (1961). Gusts at low altitude in North Africa. Ministry of Aviation, Royal Aircraft Establishment, RAE Farnborough.

Chapman, D. R. (1979). Computational aerodynamics development and outlook. AIAA journal, 17(12), 1293-1313.

Choi, H., & Moin, P. (2012). Grid-point requirements for large eddy simulation: Chapman's estimates revisited. Physics of fluids, 24 (1), 011702.

Corrsin, S. (1963). Encyclopedia of Physics. Springer. 8(2), 568.

Davidson, P. A., & Krogstad, P. Å. (2009). A simple model for the streamwise fluctuations in the log-law region of a boundary layer. Physics of Fluids, 21(5), 055105.

Dhamankar, N. S., Blaisdell, G. A., & Lyrintzis, A. S. (2015). An overview of turbulent inflow boundary conditions for large eddy simulations. In 22nd AIAA computational fluid dynamics conference. 3213.

Ektin, B. (1971). Flight in a turbulent atmosphere. In Dynamic of atmospheric flight (ed. B. Ektin), John Wiley and Sons, 547–548.

Fung Y. C. (1955).An introduction to the theory of aeroelasticity. John Wiley and Sons Inc. New York.

Jakobsen, H. A., Sannæs, B. H., Grevskott, S., & Svendsen, H. F. (1997). Modeling of vertical bubble-driven flows. Industrial & Engineering Chemistry Research, 36(10), 4052-4074.

Jiang, G., Yoshie, R., Shirasawa, T., & Jin, X. (2012). Inflow turbulence generation for large eddy simulation in non-isothermal boundary layers. Journal of Wind Engineering and Industrial Aerodynamics, 104, 369-378.

Hinze, J. O. (1975). Turbulence McGraw-Hill. New York, 218.12.

Huang, S. H., Li, Q. S., & Wu, J. R. (2010). A general inflow turbulence generator for large eddy simulation. Journal of Wind Engineering and Industrial Aerodynamics, 98(10-11), 600-617.

Hunt, J. C. R. (1973). A theory of turbulent flow round two-dimensional bluff bodies. Journal of Fluid Mechanics, 61(4), 625-706.

Issa, R. I. (1986). Solution of the Implicitly Discretised Fluid Flow Equations by Operator-Splitting, J. Comput. Phys., 62, 40–65.

Karman, T. von & Howarthl, L. (1938). Proc. R. SOC. Lond. A164, 192.

Kolmogorov, N. (1941). Dokl. Akad. Nauk. SSSR 31, 538.

Kondo, K., Murakami, S., & Mochida, A. (1997). Generation of velocity fluctuations for inflow boundary condition of LES. Journal of Wind Engineering and Industrial Aerodynamics, 67, 51-64.

Krogstad, P. A., & Davidson, P. (2011). Homogeneous turbulence generated by multi-scale grids. In *Journal of Physics: Conference Series*.318(3), 032042.

Kuethe, A. M., Willmarth, W. W., & Crocker, G. H. (1959). Stagnation point fluctuations on a body of revolution. The Physics of Fluids, 2(6), 714-716.

Larose, G. L. (1997). The dynamic action of gusty winds on long-span bridges. Denmark: Technical University of Denmark.

Lee, S., Lele, S. K., & Moin, P. (1992). Simulation of spatially evolving turbulence and the applicability of Taylor's hypothesis in compressible flow. Physics of Fluids A: Fluid Dynamics, 4(7), 1521-1530.

Li, S., Li, M., & Liao, H. (2015). The lift on an aerofoil in grid-generated turbulence. Journal of Fluid

Mechanics, 771, 16-35.

Liang, C., & Papadakis, G. (2007). Large eddy simulation of pulsating flow over a circular cylinder at subcritical Reynolds number. Computers & Fluids, 36(2), 299-312.

Li, Q.S., Xiao, Y.Q., Fu, 9.J.Y., Li, Z.N., (2007.) Full scale measurements of wind effects on the Jin Mao Building. Journal of Wind Engineering and Industrial Aerodynamics, 95, 445–466.

Lumley, J. L., & Panofsky, H. A. (1964). The structure of atmospheric turbulence. Interscience Monographs and Texts in Physics and Astronomy, New York: Wiley, 239.

Mathey, F., Cokljat, D., Bertoglio, J. P., & Sergent, E. (2006). Assessment of the vortex method for large eddy simulation inlet conditions. Progress in Computational Fluid Dynamics, an International Journal, 6(1-3), 58-67.

Mohamed, M. S., & Larue, J. C. (1990). The decay power law in grid-generated turbulence. Journal of Fluid Mechanics, 219, 195-214.

Pierce, C. D., & Moin, P. (1998). Method for generating equilibrium swirling inflow conditions. AIAA Journal, 36(7), 1325-1327.

Roberts J B, Surry D. (1973). Coherence of grid generated turbulence. Journal of the Engineering Mechanics Division, 99(6): 1227-1245.

Sadeh, W. Z., Sutera, S. P., & Maeder, P. F. (1970). Analysis of vorticity amplification in the flow approaching a two-dimensional stagnation point. Zeitschrift für angewandte Mathematik und Physik ZAMP, 21(5), 699-716.

Saffman, P. G. (1967). The large-scale structure of homogeneous turbulence. Journal of Fluid Mechanics, 27(3), 581-593.

Sankaran, R., & Jancauskas, E. D. (1993). Measurements of cross-correlation in separated flows around bluff cylinders. Journal of Wind Engineering and Industrial Aerodynamics, 49(1-3), 279-288.

Schlüter, J. U., Pitsch, H., & Moin, P. (2004). Large-eddy simulation inflow conditions for coupling with Reynolds-averaged flow solvers. AIAA Journal, 42(3), 478-484.

Simiu, E., Scanlan, R. H. (1996). Wind Effects on Structures-Fundamentals and Applications to Design. John Wiley & Sons, Inc., NewYork.

Spalart, P. R. (1986). Numerical study of sink-flow boundary layers. Journal of Fluid Mechanics, 172, 307-328.

Spalart, P. R. (1988). Direct simulation of a turbulent boundary layer up to R θ=1410. Journal of Fluid Mechanics, 187, 61-98.

Sutera, S. P. (1965). Vorticity amplification in stagnation-point flow and its effect on heat transfer. Journal of Fluid Mechanics, 21(3), 513-534.

Tabor, G. R., & Baba-Ahmadi, M. H. (2010). Inlet conditions for large eddy simulation: a review. Computers & Fluids, 39(4), 553-567.

Taylor, G. I. (1935). Statistical theory of turbulence. In Proceedings of the Royal Society of London A: Mathematical, Physical and Engineering Sciences. The Royal Society. 151(873), 421-444.